

## Rheological Behavior

The flow behavior of PAN and BA solutions in the needles during the electrospinning could be identified through rheology. Figure I displays the shear stress and viscosity as a function of the shear rate for the PAN/DMF solution (PAN loading: 8, 9, 10, 11, or 12 wt%) and the BA liquid. Figure Ia reveals the effect of shear stress with respect to the shear rate for these samples. At lower shear rates ( $< 1 \text{ s}^{-1}$ ), the motion of the BA monomer was highly unstable, due to the predominately molecular interactions. When the shear rate increased beyond  $1 \text{ s}^{-1}$ , the shear stress of BA increased linearly. In addition, the shear stress increased exponentially upon increasing the polymer mass fraction, because the polymer solution became thicker accordingly. For a non-Newtonian fluid, the orientation of the polymer chains is the governing factor that influences the fluid behavior [1]. The rheology of a non-Newtonian fluid is often described by the power law equation

$$\tau = K\gamma^n \quad (1)$$

where  $\tau$  is the shear stress,  $K$  is the flow consistency index,  $\gamma$  is the shear rate, and  $n$  is the flow behavior index. The larger the deviation of  $n$  from 1, the more non-Newtonian is the behavior of the fluid. For a Newtonian fluid,  $n$  is equal to 1; for a dilatant,  $n$  is greater than 1; for a pseudoplastic fluid,  $n$  is less than 1 [2,3]. Table I summarizes the values of  $n$ ,  $K$ , and  $R^2$  (statistical correlation coefficient). The values

of  $n$  for our PAN/DMF samples were all less than 1, indicating the pseudoplastic nature of these solutions. Upon increasing the concentration of PAN, the value of  $n$  decreased, revealing more-obvious pseudoplastic behavior; accordingly, the solutions exhibited greater shear thinning phenomena (the viscosity decreased nearly linearly upon increasing the shear rate; Figure Ib). The viscosity and shear stress of the 12 wt% PAN/DMF solution were much larger than those of the other PAN/DMF solutions, indicating predominantly pseudoplastic behavior. The orientation of the macromolecular chains was the major cause of such non-Newtonian behavior. Upon increasing the shear rate, the number of oriented polymer segments increased, thereby decreasing the viscosity of the 12 wt% PAN solution, greatly increasing its non-Newtonian behavior [4]. Thus, the great decrease in viscosity of the PAN solution at larger shear rates was due primarily to the orientation of the polymer segments. For the BA solution, the value of  $n$  suggested behavior approaching that of a Newtonian fluid (see Table I, which also lists the flow consistency index  $K$  and values of  $R^2$ ).

The solution viscosity (an indicator of polymer concentration) and solution surface tension play important roles in determining the morphology of electrospun nanofibers. We approximated the apparent shear rate at the respective needle walls by considering the solutions as Newtonian fluids and applying equation (2):

$$\gamma' = \frac{4Q}{\pi R^3} \quad (2)$$

where  $\gamma'$  is the apparent shear rate at the needle wall,  $Q$  is the volumetric flow rate, and  $R$  is the radius of the needle (255  $\mu\text{m}$  for the inner needle; 685  $\mu\text{m}$  for the outer needle). Figure Ib reveals the effect of the viscosity of these solutions at various shear rates. For a typical flow rate of 0.5  $\text{mL h}^{-1}$ , the calculated shear rates were approximately 0.8 and 9  $\text{s}^{-1}$  at the two respective needle walls; these values are illustrated by the dotted lines in Figure Ib. The viscosity curves in Figure Ib indicate that the solutions were nearly Newtonian at these operating shear rates in the coaxial needle, supporting the use of Eq 1. All of the solutions exhibited well-developed zero-shear viscosity plateaus between shear rates of 0.8 and 9  $\text{s}^{-1}$ . Shear-thinning occurred at lower shear rates; this behavior was amplified upon increasing the polymer content because of greater disentanglement of polymer chains. The shear-thinning of the PAN solutions was much greater than that of the BA liquid, indicative of a larger characteristic time. Considering the above rheology, the optimal inner and outer flow rates for producing uniform core/shell fibers were 1 and 10  $\text{mL h}^{-1}$ , respectively.

[1] Grabowski, D. A.; Schmidt, C.; Simultaneous Measurement of Shear Viscosity and Director Orientation of a Side-Chain Liquid-Crystalline Polymer by Rheo-NMR, *Macromolecules*. 1994, 27, 2632–2634.

[2] Scott. Blair, G. W.; Hening, J. C.; Wagstaff, A.; The Flow of Cream through Narrow Glass Tubes, *J. Phys. Chem.* 1939, 43, 853–864.

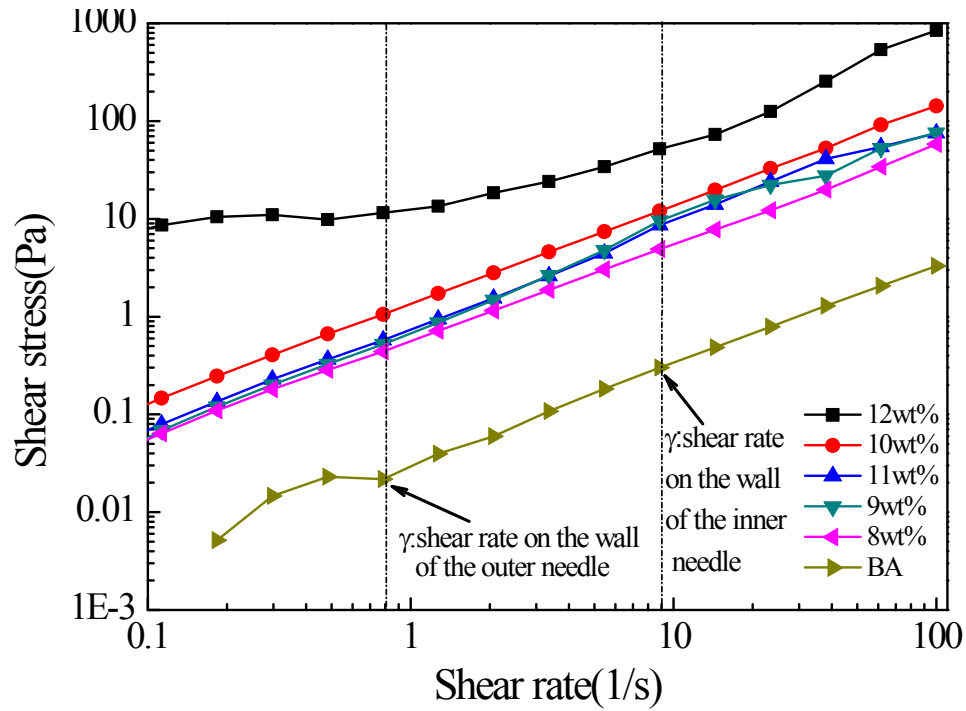
- [3] Zhang, D.; Karki, A. B.; Rutman, D.; Young, D. P.; Wang, A.; Cocke, D.; Ho, T. H.; Guo, Z.; Electrospun polyacrylonitrile nanocomposite fibers reinforced with Fe<sub>3</sub>O<sub>4</sub> nanoparticles: Fabrication and property analysis, *Polymer*. 2009, 50, 4189–4198.
- [4] Liu, W.; Cheng, L.; Zhang, H.; Zhang, Y.; Wang, H.; Yu, M.; Rheological Behaviors of Polyacrylonitrile/1-Butyl-3-Methylimidazolium Chloride Concentrated Solutions, *Int. J. Mol. Sci.* 2007, 8, 180–188.

Table I Rheological data of PAN solutions and BA

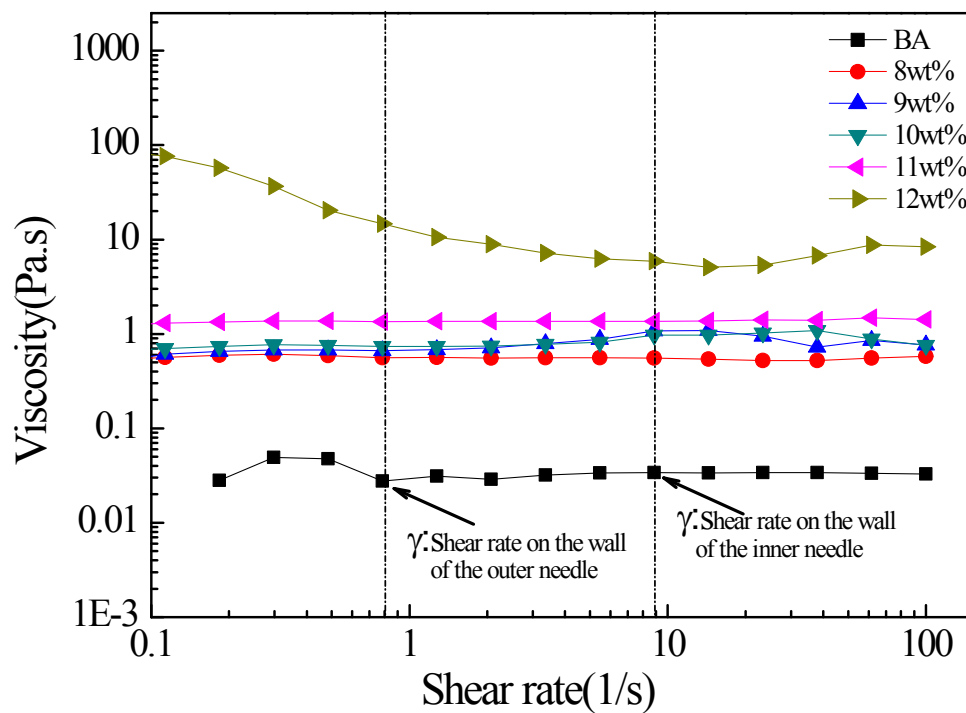
solution	$k$	$n$	$R^2$
BA liquid	0.01	0.94	0.9999
8 wt% PAN solution	0.14	0.90	0.9993
9 wt% PAN solution	0.27	0.88	0.9879
10 wt% PAN solution	0.81	0.85	0.9998
11 wt% PAN solution	0.19	0.83	0.9997
12 wt% PAN solution	7.1	0.80	0.9797

Figure I: Rheological behavior of BA liquid and PAN solutions. (a) Shear stress; (b) viscosity plotted with respect to shear rate.

(a)



(b)



Static water contact angles (SWCAs) were measured by increasing the drop volume and recording the angle on a GH-100 contact angle system (Krüss). The SWCAs were determined by fitting a Young–Laplace curve around the drop. The experiment was performed under normal laboratory ambient conditions at 35% relative humidity. The mean value was calculated from at least 10 individual measurements. The earliest modeling studies of liquid drops on rough surfaces were performed by Wenzel [5] and Cassie [6]. Their models are described using the following equations:

$$\cos \theta_r = r \cos \theta_s \quad (3)$$

$$\cos \theta_r = f_1 \cos \theta_s - f_2 \quad (4)$$

where  $\theta_r$  and  $\theta_s$  are the equilibrium (Young's) SWCAs of a rough surface and a smooth surface, respectively, and  $f_1$  and  $f_2$  are the fractions of a solid surface and air in contact with a liquid droplet, respectively ( $f_1 + f_2 = 1$ ). Eq. (4) assumes that the liquid does not completely wet the rough surface. Once air is trapped in the interstices of the rough surface, the liquid droplet interacts with the composite surface, which consists of the solid substrate and air pockets.

We used eqns (3) and (4) to calculate the fractions of the solid surface ( $f_1$ ) and air ( $f_2$ ) in contact with the liquid droplets (Table 2). The values of  $f_1$  and  $f_2$  correlated directly to the SWCAs. The effect of the polymer concentration on the SWCA was significant.

For example, the values of  $f_1$  decreased from 0.284 to 0.059 upon increasing the PAN concentration from 8 to 12%. Curing of the electrospun membranes did not lead to significant changes in either  $f_1$  or  $f_2$ , indicating that the structures of the PAN-BA fibrous mats remained intact after curing.

[5] Wenzel, R. N.; A new methodology for the optimal design and production schedule of multipurpose batch plants, *Ind. Eng. Chem.* 1936, 28, 988.

[6] Cassie, A. B. D.; Baxter, S.; Wettability of porous surfaces, *Trans. Faraday Soc.* 1944, 40, 546.

Table II SWCAs and fractional interfacial areas of solid and air contact with a water droplet for PAN-BA and PAN-PBA samples prepared through spin-coating and coaxial electrospinning

sample	SWCA (°)		fraction of solid contact with a water droplet ( $f_1$ )	fraction of air contact with a water droplet ( $f_2$ )
	spin-coating	electrospinning		
P8-BA	44 ± 3	121 ± 3	0.284	0.716
P9-BA	46 ± 3	125 ± 3	0.249	0.75
P10-BA	45 ± 2	130 ± 4	0.209	0.791
P11-BA	43 ± 3	136 ± 4	0.164	0.835
P12-BA	44 ± 3	154 ± 5	0.059	0.941
P8-PBA	71 ± 3	127 ± 3	0.30	0.70
P9-PBA	68 ± 3	129 ± 3	0.276	0.723
P10-PBA	70 ± 4	135 ± 3	0.218	0.781
P11-PBA	69 ± 3	145 ± 4	0.135	0.865
P12-PBA	72 ± 3	158 ± 5	0.054	0.945

